

## A method for quality management of vegetation phenophases derived from satellite remote sensing data

Yongjian Ruan, Xinchang Zhang, Qinchuan Xin, Ying Sun, Zurui Ao & Xin Jiang

To cite this article: Yongjian Ruan, Xinchang Zhang, Qinchuan Xin, Ying Sun, Zurui Ao & Xin Jiang (2021) A method for quality management of vegetation phenophases derived from satellite remote sensing data, International Journal of Remote Sensing, 42:15, 5801-5820, DOI: [10.1080/01431161.2021.1931534](https://doi.org/10.1080/01431161.2021.1931534)

To link to this article: <https://doi.org/10.1080/01431161.2021.1931534>



Published online: 23 Jun 2021.



Submit your article to this journal



View related articles



View Crossmark data



# A method for quality management of vegetation phenophases derived from satellite remote sensing data

Yongjian Ruan<sup>a,b</sup>, Xinchang Zhang<sup>a,c</sup>, Qinchuan Xin<sup>c,d</sup>, Ying Sun<sup>b</sup>, Zurui Ao<sup>b</sup> and Xin Jiang<sup>b</sup>

<sup>a</sup>School of Geography and Remote Sensing, Guangzhou University, Guangzhou, China; <sup>b</sup>School of Geography and Planning, Sun Yat-Sen University, Guangzhou, China; <sup>c</sup>The College of Environment and Planning of Henan University, Henan University, Kaifeng, China; <sup>d</sup>State Key Laboratory of Desert and Oasis Ecology, Research Center for Ecology and Environment of Central Asia, Chinese Academy of Sciences, Urumqi, China

## ABSTRACT

Remote sensing has become an important technique for monitoring vegetation phenology. The quality of remote-sensing images and derived products is key to successful extraction of vegetation phenophases. There is a need to develop quality management methods to evaluate the data uncertainty and assist the removal of the noises. This paper developed a shape quality assurance score threshold (SQAT) method which accounts for the trend in satellite-derived vegetation index associated with the process of vegetation growth. The proposed method was tested on six widely used methods for extracting vegetation phenophases. Results showed that the SQAT method can effectively identify noises in the vegetation index time series and improve the accuracies of estimated start of season (SOS) and end of season (EOS) of the six methods. After removal of identified noises, the Pearson correlation coefficient ( $r$ ) averagely increased by 8% for SOS, and 11% for EOS. Regression analyses of vegetation phenophases between the PhenoCam observations and MCD12Q2 product showed that the proposed method performs better than the QA score of MCD12Q2 for quality management. This paper provides promising method for quality management; it has the potential to reduce the uncertainty of the vegetation index time series that can support studies of vegetation phenology monitoring.

## ARTICLE HISTORY

Received 25 September 2020  
Accepted 11 May 2021

## 1. Introduction

Vegetation phenology, the recurring biological events throughout the year, have a profound impact on the physical and biogeochemical processes of vegetation (Myneni et al. 1997), the carbon balance of natural systems (Piao et al. 2007), and the climate–vegetation interaction (Richardson et al. 2013). Studies have used ecological models (Xin, Dai, and Liu 2019; Xin et al. 2015; Lucht et al. 2002), ground-based observations (Ge et al. 2015; Fu et al. 2015; Richardson et al. 2018), and satellite remote sensing images (Zhou et al. 2016; Yu et al. 2003; Sakamoto et al. 2005; Tan et al. 2011; Piao et al.

2006; Zhang et al. 2003) to retrieve vegetation phenophases for analysis. Among them, satellite remote sensing has rich historical data and suitable spatial and temporal resolution, and it has become an important technology for estimating and monitoring vegetation phenophases on a large regional scale.

Many vegetation phenophase estimation methods based on satellite remote sensing data have been developed to produce regional- or global-scale phenological products, such as the amplitude threshold (AT) (Fischer 1994; Zhou et al. 2016), first-order derivative (FOD) (Yu et al. 2003), second-order derivative (SOD) (Sakamoto et al. 2005), third-order derivative (TOD) (Tan et al. 2011), relative change rate (RCR) (Piao et al. 2006), and curvature change rate (CCR) (Zhang et al. 2003). These methods provide basic algorithms for satellite remote sensing vegetation phenology research. In the past, there were few ground-based observational records of vegetation phenophases publicly released online, so it was difficult for researchers to obtain ground validation data to evaluate the reliability of methods (Zhou et al. 2016). Besides, researchers paid more attention to phenological metric estimation methods (Hufkens et al. 2018), and focused less on how to control and measure the quality of the estimated results. Typically, researchers often used a simple threshold method to control the quality of the estimated results; for instance, the start of season (SOS) values  $<30$  and  $>185$  and the end of season (EOS) values  $<185$  and  $>330$  are directly removed (Li et al. 2017; Ruan et al. 2019; Zhou et al. 2016). However, the threshold-based method may not be the best, as it is usually dependent on the ecosystem studied and hard to generalize.

Affected by complex atmospheric and ground conditions such as clouds, rain, and snow/ice cover (Wang, Xie, and Liang 2008; Jun et al. 2005), the optical satellites cannot avoid capturing noise (other reflectance) that disrupts useful information (vegetation reflectance). Therefore, the quality management method is significant for achieving accurate estimation results. Especially in publicly released products, it is crucial to eliminate the results of estimation from noisy remote sensing time series data to improve the accuracy and reduce the uncertainty of the estimated phenophases, which can then be better used for vegetation phenology research. The MCD12Q2 product has a Quality assurance (QA) scores layer (Friedl, Gray, and Sulla-Menashe 2019), and the scores are divided into four categories to describe the quality of the products. The QA score of MCD12Q2 accounts for the missing (e.g. due to snow) and the filled (e.g. with dormant nbar-evi2 value) pixels and the goodness of fit of smoothing spline models. However, it does not consider the process of vegetation growth to evaluate the quality of satellite-derived vegetation index. And to the best of our knowledge, no related research has used in-situ data to evaluate the effectiveness of MCD12Q2 QA scores. Overall, there is a need to develop the quality management method for satellite-retrieved vegetation phenophases.

Recently, some vegetation phenological datasets acquired from ground-based observations were released on the Internet, such as the Pan European Phenological database (PEP725) (Templ et al. 2018), the USA National Phenology Network (USA-NPN) data resources, and the PhenoCam Dataset (Seyednasrollah et al. 2019). PEP725 and USA-NPN were collated mainly by human observations, and the PhenoCam Dataset mainly employs conventional red-green-blue (RGB) digital cameras and provides an alternative to human observations. While recording the timing of the specific phenophases of plants, the cameras can decrease the uncertainty caused by nonuniformity compared to



traditional human observations (Menzel 2002; Richardson et al. 2018). The cameras also have other advantages (Sonnentag et al. 2012), including low cost and ease of obtaining spectral information of plants with high temporal frequency.

In this paper, we employed the PhenoCam Dataset, MOD09Q1, and MCD12Q2 to investigate the performance of six methods for estimating vegetation phenophases and developed a shape quality assurance score threshold (SQAT) method for quality management of the estimated results.

## 2. Materials

### 2.1. MODIS data

We employed the MODIS/Terra surface reflectance 8-day 250 m product (MOD09Q1, Version 6) from 2009 to 2018 in the conterminous United States as the research data (Vermote 2015), which is available from <https://search.earthdata.nasa.gov/>. These data include two surface reflectance bands (red band, 620–670 nm; near-infrared band, 841–876 nm) and are widely used for extracting the two-band enhanced vegetation index (EVI2) (Ruan et al. 2019; Yang et al. 2012). The EVI2 time series data can be derived from the surface reflectance bands in MOD09Q1 as follows (Jiang et al. 2008):

$$\text{EVI2} = 2.5 \frac{\rho_N - \rho_R}{\rho_N + 2.4\rho_R + 1} \quad (1)$$

The MODIS/Terra and Aqua Land Cover Dynamics Yearly L3 Global 500 m SIN Grid (MCD12Q2, Version 6), which provides vegetation phenophases over global land surfaces from 2001 to 2017 (Friedl, Gray, and Sulla-Menashe 2019), is also available from <https://search.earthdata.nasa.gov/>. The MCD12Q2 product was derived from the EVI2 time series which were calculated from MODIS nadir bidirectional reflectance distribution function (BRDF)-adjusted reflectance (NBAR). We used the greenup layer, the dormancy layer, and the QA detailed layer of MCD12Q2 from 2009 to 2017 in the conterminous United States as auxiliary data to verify the effectiveness of the proposed algorithm. In the MCD12Q2 product, the pixel value of the greenup layer (i.e. SOS) and the dormancy layer (i.e. EOS) is acquired from the date when EVI2 reaches the first and last 15% of the maximum values, respectively. The QA score in MCD12Q2 is a weighted combination of two fractions, i.e. the fraction of not missing (e.g. due to snow) and not filled (e.g. with dormant NBAR-EVI2 value) values (80% weight), and the goodness-of-fit ( $R^2$ ; 20% weight) of the spline models for the EVI2 values within 2 weeks around the key phenophases (Friedl, Gray, and Sulla-Menashe 2019). The QA scores of MCD12Q2 were divided into four classes, namely, best (0), good (1), fair (2), and poor (3), and more details can be found at <https://lpdaac.usgs.gov/products/mcd12q2v006/>. In this paper, we used the best level threshold of the QA scores from MCD12Q2 (MCDQAT) to control the quality of vegetation phenophases.

### 2.2. PhenoCam Dataset

The ground-based observational vegetation phenology records from the PhenoCam Dataset v2.0 (Richardson et al. 2019) were obtained (<https://phenocam.sr.unh.edu/webcam/>) for validation. The PhenoCam was established in 2008 and includes approximately

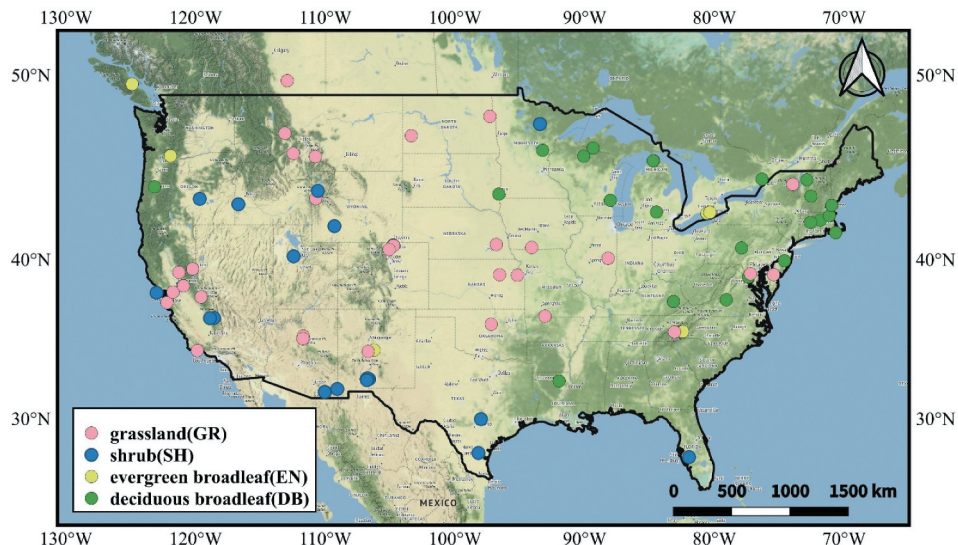


**Figure 1.** Locations of the selected deciduous broadleaf (DB), evergreen broadleaf (EN), shrub (SH), and grassland (GR) PhenoCam sites.

500 sites which were concentrated in North America. In these sites, digital camera networks were used to track vegetation phenology. In this paper, we employed 117 PhenoCam sites from 2009 to 2018 for analysis (as shown in Figure 1), which included 28 deciduous broadleaf (DB) sites, 9 evergreen broadleaf (EN) sites, 42 shrub (SH) sites, and 38 grassland (GR) sites. We used the DB, EN, SH, and GR PhenoCam sites for satellite-retrieved SOS validation, and the DB, SH, and GR PhenoCam sites for satellite-retrieved EOS validation, respectively. The vegetation phenophases of the PhenoCam Dataset were extracted according to the green chromatic coordinate index ( $G_{cc}$ ) change (Richardson et al. 2018) in the region of interest (ROI) of a specific vegetation type. In the PhenoCam Dataset, three threshold values (i.e. 10%, 25% and 50%) of  $G_{cc}$  were used to identify vegetation phenophases. Note that the threshold value 50% of vegetation index time series is rarely used to retrieve vegetation phenophases from remote sensing data, and the SOS and EOS retrieved by threshold values of 10% and 25% of vegetation index time series are similar (as shown Figure 2). Therefore, we selected the SOS and EOS, which were retrieved from the threshold values of 25% of mean  $G_{cc}$  amplitude for analysis.

### 3. Methodology

#### 3.1. Methods of extracting vegetation phenophases

We tested six methods for estimating vegetation phenophases, as shown in Table 1. These six methods are widely used to estimate the SOS and EOS from satellite time series data such as EVI, EVI2, NDVI, and LAI. The raw vegetation index time series data usually need to be pre-processed before estimating phenophases. The SOS and EOS of vegetation generally occurs from 1 to 365 days in the Northern Hemisphere. Therefore, for the convenience of calculation, we linearly interpolate the 8-day EVI2 time series into daily time

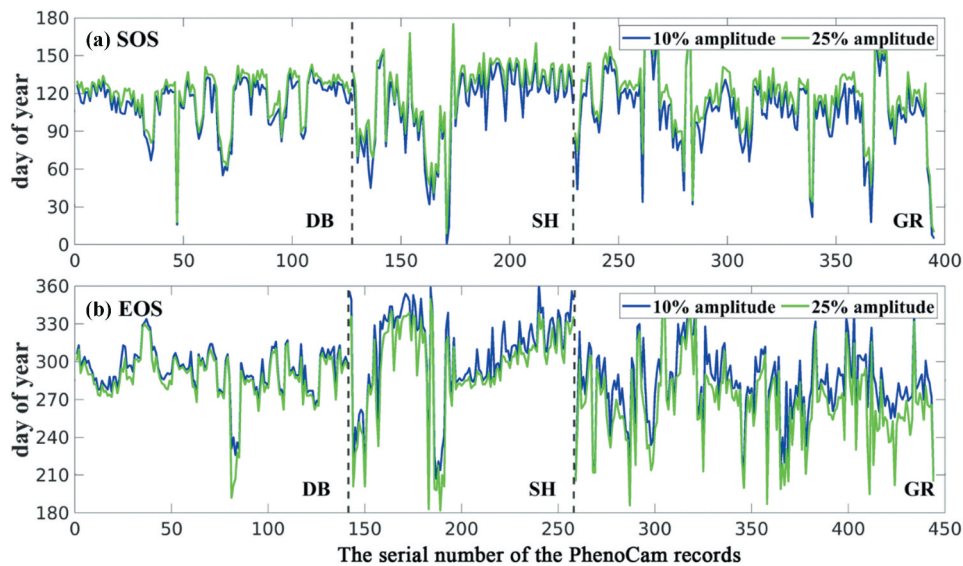


**Figure 2.** Comparison of phenological metrics including start of season (SOS) and end of season (EOS) acquired from PhenoCam observatory data extracted by 10% and 25% amplitude threshold of the green chromatic coordinate index ( $G_{cc}$ ).

**Table 1.** Description of the six methods for extracting vegetation phenophases (i.e. start of season (SOS) and end of season (EOS)).

Method	Name in this paper	SOS	EOS	Reference
Amplitude threshold	AT	$0.2 \times (\max(EVI2_s) - \min(EVI2_s))$	$0.2 \times (\max(EVI2_a) - \min(EVI2_a))$	(Zhou et al. 2016)
First-order derivative	FOD	$\max(dt(EVI2_s))$	$\min(dt(EVI2_a))$	(Yu et al. 2003)
Second-order derivative	SOD	$\max(dt^2(EVI2_s))$	$\max(dt^2(EVI2_a))$	(Sakamoto et al. 2005)
Relative change rate	RCR	$\max\left(\frac{EVI2_s(t+1)-EVI2_s(t)}{EVI2_s(t)}\right)$	$\min\left(\frac{EVI2_a(t+1)-EVI2_a(t)}{EVI2_a(t)}\right)$	(Piao et al. 2006)
Third-order derivative	TOD	$\max(dt^3(EVI2_s))$	$\min(dt^3(EVI2_a))$	(Tan et al. 2011)
Curvature change rate	CCR	$\max(K'_s(t))$	$\max(K'_a(t))$	(Zhang et al. 2003)

Note: where  $EVI2_s$  represents EVI2 at the time of vegetation growth (i.e. spring);  $EVI2_a$  represents EVI2 at the time of vegetation dormancy (i.e. autumn);  $t$  represents the day of the year in the EVI2 time series;  $K'_s$  represents the rate of change of curvature of the logistic-fitted EVI2 time series during the time of vegetation growth (i.e. spring);  $K'_a$  represents the rate of change of curvature of the logistic-fitted EVI time series during the time of vegetation dormancy (i.e. autumn) (for more details, please see (Zhang et al. 2003));  $\max()$  and  $\min()$  denote obtaining the maximum and minimum values of the time series data, respectively; and  $dt()$ ,  $dt^2()$ , and  $dt^3()$  denote obtaining the first-order, second-order, and third-order derivatives of time series data, respectively.

series, and then used the Savitzky–Golay (S-G) method (Savitzky and Golay 1964) to remove the outliers.

The growing season was divided into growth (i.e. spring) and dormancy (i.e. autumn) periods, and a logistic function (as shown in equation 2) was used to fit EVI2 values in each period.

$$y(t) = \frac{c}{1 + e^{a+bt}} + d \quad (2)$$

where  $y(t)$  denotes the EVI2 value at time  $t$ ;  $t$  denotes the day of the year;  $a$ ,  $b$ , and  $c$  are the fitting parameters; and  $d$  is the minimum value of the EVI2 time series. We sorted the data series data by day of the year in descending order (365<sup>th</sup> to 1<sup>th</sup>) when fitting the EVI2 of vegetation dormancy with equation (2).

### 3.2. The SQAT quality control method

In this paper, we propose a shape quality assurance score threshold (SQAT) method for quality management of the vegetation phenophases extracted by the six methods. The method includes two steps. In the first step, a shape quality assurance (SQA) score is developed. Whereas in the second step, the high-quality vegetation phenophases were selected according to the threshold of SQA. To keep consistent with the MCD12Q2 QA method (Friedl, Gray, and Sulla-Menashe 2019), we set the SQA threshold to 0.75. The main idea behind SQA is to improve the MCD12Q2 QA method by further considerations on the trends in satellite-derived vegetation index associated with the process of vegetation growth. The SQA score is calculated as follows.

- (a) We calculated the R squared ( $R^2$ ) of regression analysis between the daily EVI2 time series and the smoothed daily EVI2 time series (i.e. S-G) in the quality assurance (QA) window for estimating the goodness-of-fit of spline models (as shown in the Figure 3b). The QA window is referring to the MCD12Q2 QA scores (Friedl, Gray, and Sulla-Menashe 2019), and it is defined as 2 weeks before and after the vegetation phenophase (i.e. SOS and EOS) (Friedl, Gray, and Sulla-Menashe 2019) (as shown in Figure 3a). The equation is as follows:

$$Q_R = R^2 \quad (3)$$

To keep in line with the MCD12Q2 QA scores, we set the size of the time window as 2 weeks around the vegetation phenophases.

b. We counted the number of bad-quality pixels (i.e. cloud, sown, and filled pixels), and calculated the proportion of good-quality pixels in the eight-day EVI2 time series (Friedl, Gray, and Sulla-Menashe 2019) (as shown in the embedded subplot of Figure 3a). Note that the snow pixels are bad quality pixels in monitoring vegetation reflectance, as remote sensors will capture the snow reflectance instead of the vegetation reflectance if snow covers the vegetation. The equation is as follows:

$$Q_p = (1 - n/N) \quad (4)$$

where  $n$  denotes the number of bad-quality pixels, and  $N$  ( $N = 46$ ) denotes the number pixels of the EVI2 time series.

c. Generally, the growth cycle of vegetation consists of three irreversible processes, that is, germination, maturation, and senescence. Due to the physiological and biochemical changes during growth, EVI2 tends to increase from germination to maturation, and decrease from maturation to senescence. We assumed that the abnormal situation is caused by data quality problems, and estimated the consistency between the shape of

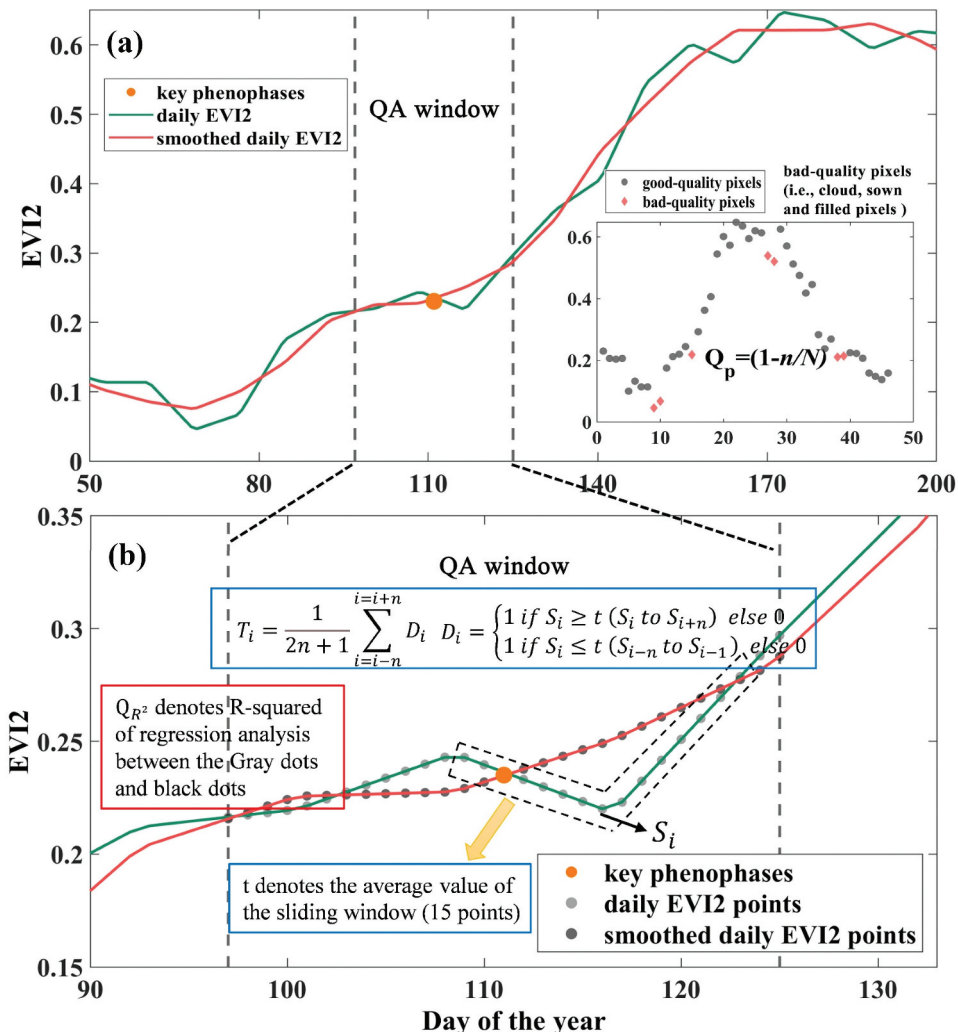


**Figure 3.** An illustration of how the SQA score was calculated from time series of EVI2. (a) the define of QA window in the EVI2 time series and the good-quality pixels ratio was calculated from the EVI2 time series; (b) the window of the EVI2 time series used to calculate phenometric-specific QA scores. EVI2, the two-band enhanced vegetation index; QA, quality assurance; SQA, shape quality assurance.

EVI2 time series and the growth trends to provide a measurement for the quality of vegetation phenophases. A neighbourhood probability method proposed by (Latifovic and Pouliot 2007) was used to estimate whether the shape of EVI2 time series conforms to the process of vegetation growth. This method has proved to be effective in dealing with both the vegetation index and the lake ice brightness temperature time series (Ruan et al. 2016, 2019; Latifovic and Pouliot 2007; Weber et al. 2016). Considering the difference between the lake ice phenology profile and vegetation phenology profile, we slightly adjusted the equation from the original reference (Latifovic and Pouliot 2007). The modified method is shown in equation 5. The equation (6) was used to calculate

a robust trend of the normal vegetation growth in the QA window (as shown in the [Figure 3b](#)). The equations are as follows:

$$T_i = \frac{1}{2n+1} \sum_{i=i-n}^{i=i+n} D_i D_i = \begin{cases} 1 & \text{if } S_i \geq t(S_i \text{ to } S_{i+n}) \text{ else } 0 \\ 1 & \text{if } S_i \leq t(S_{i-n} \text{ to } S_{i-1}) \text{ else } 0 \end{cases} \quad (5)$$

$$Q_t = \frac{1}{29} \sum_{i=d-14}^{i=d+14} T_i \quad (6)$$

In equation 5,  $n$  ( $n = 7$ ) denotes the sliding window size,  $t$  denotes the average EVI2 of all points in the sliding window, and  $S_i$  denotes the value of  $i^{\text{th}}$  point in the EVI2 time series. Due to vegetation growth is irreversible, the EVI2 was expected to monotonously increase in the time period of vegetation greenup. Therefore, for EVI2 values from  $i$  to  $i + n$ ,  $S_i \geq t$  is normal ( $D_i=1$ ), and  $S_i < t$  is abnormal ( $D_i=0$ ). Similarly, for EVI2 values from  $i-n$  to  $i-1$ ,  $S_i \leq t$  is normal ( $D_i=1$ ), and  $S_i > t$  is abnormal ( $D_i=0$ ). And the condition of vegetation dormancy is opposite. We calculated the  $D_i$  from the 15 points of the sliding window, and used the average value of those as  $T_i$ . Finally, the equation 6 was used to calculate the average value of all  $T_i$  in QA window to estimate the data quality of the EVI2 time series in QA window.

d. The SQA score was calculated by a combination of  $Q_p$ ,  $Q_R$ , and  $Q_t$  by the following formula:

$$SQA = 0.2 \times Q_{R^2} + 0.3 \times Q_p + 0.5 \times Q_t \quad (7)$$

Where 0.2, 0.3 and 0.5 in equation (7) are the weights. The weight of  $Q_{R^2}$  is in line with that of MCD12Q2 QA scores (Friedl, Gray, and Sulla-Menashe [2019](#)). Considering the importance of the shape of the input EVI2 time series in satellite-retrieved phenophases, we assigned 0.5 of the remaining 0.8 weight to  $Q_t$ , and then assigned last 0.3 weight to  $Q_p$ .

### 3.3. Method evaluation

This paper used the metrics of the Pearson correlation coefficients and the normalized root-mean-square error (NRMSE) for method evaluation (Kuklisova-Murgasova et al. [2012](#)). NRMSE is a normalized metric which can make a better model evaluation than the mean absolute error (MAE) and the root-mean-square error (RMSE) in the comparison of two groups that have different sample sizes. The NRMSE is calculated as follows:

$$NRMSE = \frac{\sqrt{\sum_{i=1}^N (\hat{y}_i - y_i)^2 / N}}{\sum_{i=1}^n y_i / N} \quad (8)$$

where  $N$  is the number of samples,  $\hat{y}_i$  is the satellite-retrieved phenophases of sample  $i$ ,  $y_i$  is the PhenoCam-observed phenophases of sample  $i$ .

## 4. Results

### 4.1. Analysis of the SQAT effectiveness at the site scale

We selected four types of vegetation (i.e. DB, EN, SH, and GR) from the near-surface remote-sensing observation network as validation data for the satellite-retrieved SOS. [Figure 4](#)



illustrates the regression analysis between the SOS estimated from the MOD09Q1 EVI2 time series six methods (y-coordinate) and the SOS obtained from the PhenoCam Dataset (x-coordinate). The SOS retrieved from six methods (i.e. AT, FOD, SOD, RCR, TOD, and CCR) achieved r values of 0.59, 0.58, 0.58, 0.56, 0.53 and 0.55, the normalized root mean squared error (NRMSE) values of 0.24, 0.23, 0.26, 0.23, 0.36 and 0.35, respectively. After using SQAT for quality management, the obtained SOS achieved r values of 0.65, 0.61, 0.67, 0.58, 0.65 and 0.72, and NRMSE values of 0.22, 0.22, 0.24, 0.23, 0.35 and 0.33, respectively. It can be observed that the r value was significantly improved and the NRMSE value decreased.

[Figure 5](#) illustrates the regression analysis between the EOS estimated from the MOD09Q1 EVI2 time series by the six methods (y-coordinate) and the EOS obtained from the PhenoCam Dataset (x-coordinate). The EOS from the methods of AT, FOD, SOD, RCR, TOD and CCR achieved r values of 0.65, 0.68, 0.65, 0.65, 0.38 and 0.41, NRMSE values of 0.17, 0.16, 0.17, 0.16, 0.23 and 0.22, respectively. After using SQAT for quality management, the obtained EOS achieved r values of 0.75, 0.71, 0.73, 0.74, 0.58 and 0.57, and NRMSE values of 0.14, 0.16, 0.15, 0.13, 0.20 and 0.20, respectively. As shown in [Figure 5](#), a better result was yielded while using SQAT for quality management.

In addition, we employed the vegetation phenophases (i.e. SOS and EOS) from MCD12Q2 to verify the effectiveness of the SQAT method. The spatial resolution of MCD12Q2 is 500 m, and the MOD09Q1 data were used to calculate the SQA scores with a spatial resolution of 250 m. They are obtained from the same sensor (MODIS), so we assumed that they were consistent with the scale observed in the PhenoCam Dataset. We directly applied the SQA scores calculated by the AT in [Section 4.1](#) for quality management of the MCD12Q2 phenophases, and then conducted regression analysis with the vegetation phenophases from the PhenoCam Dataset. The scatterplots shown in [Figure 6](#) compare the SOS obtained from PhenoCam Dataset and MCD12Q2. The regression analysis indicated that the original SOS of MCD12Q2, the SOS of MCD12Q2 with MCDQAT for quality management, and the SOS of MCD12Q2 with SQAT for quality management achieved r values of 0.42, 0.50 and 0.56, NRMSE values of 0.25, 0.21 and 0.20, respectively. Comparisons of the three results demonstrated that SQAT quality management method effectively improved the accuracy of retrieved SOS.

[Figure 7](#) shows scatterplots for the EOS obtained from MCD12Q2 and the PhenoCam Dataset. The regression analysis indicated that the original EOS of MCD12Q2, the EOS of MCD12Q2 with MCDQAT for quality management, and the EOS of MCD12Q2 with SQAT for quality management achieved r values of 0.64, 0.66 and 0.73, NRMSE values of 0.17, 0.17 and 0.16, respectively. Among them, using SQAT for quality management of the EOS achieved the best results.

#### 4.2. Analysis of the SQAT effectiveness at the regional scale

To evaluate the performance of SQAT at a regional scale, we selected vegetation phenophases extracted by AT and FOD (the first and second methods) for comparison with the MCD12Q2 phenophases. [Figure 8](#) shows the spatial distribution of SOS in 2017 as derived from the MOD09Q1 data and acquired from the MCD12Q2 product in the conterminous United States. The MCDQAT method ([Figure 8b](#)) and SQAT method ([Figure 8d](#), [Figure 8f](#)) were used to optimize the SOS mapping. Both MCDQAT and SQAT methods could remove outlier pixels in the original result and improve the spatial distribution. Comparing with

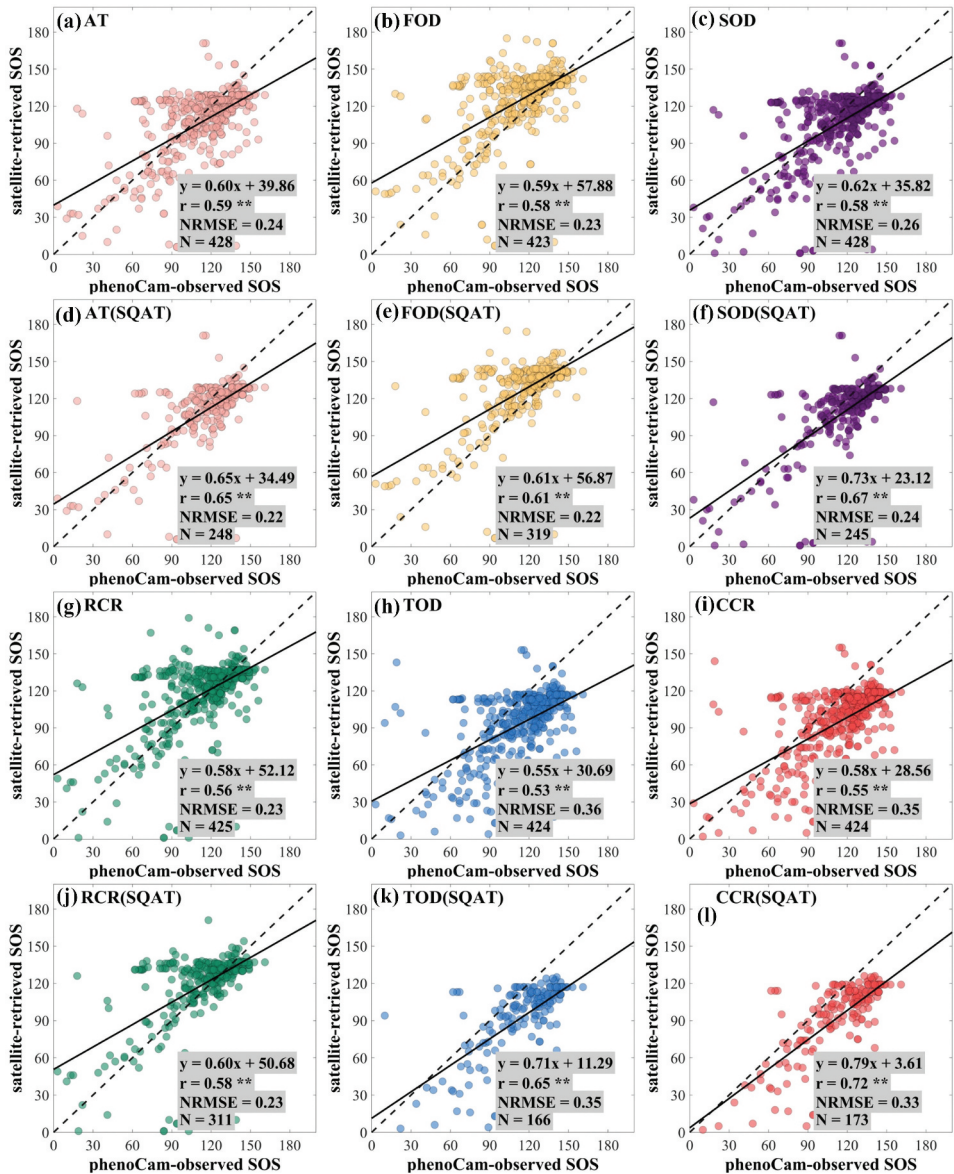


**Figure 4.** Scatterplots for the regression analysis between the PhenoCam-observed and the satellite-retrieved SOS using the methods of: (a) Amplitude threshold (AT); (b) first-order derivative (FOD); (c) second-order derivative (SOD); (d) AT and the shape quality assurance score threshold (SQAT); (e) FOD and SQAT; (f) SOD and SQAT; (g) relative change rate (RCR); (h) third-order derivative (TOD); (i) curvature change rate (CCR); (j) RCR and SQAT; (k) TOD and SQAT; and (l) CCR and SQAT. SQAT denotes use of the SQAT method for quality management of the satellite-retrieved SOS. \*\* denotes a  $p$ -value of two-tailed Student's  $t$ -tests of  $<0.01$ .  $N$  denotes the number of validation sites.

**Figure 8a**, the MCDQAT method shows a decrease in low-value (green) pixels near Washington, Idaho, and Montana, and high-value (red) pixels near Colorado in **Figure 8b**. Using the SQAT method, the SOS maps in **Figure 8d** and **Figure 8f** have a significantly reduced number of low-value (green) pixels near California and Texas and high-value (red)

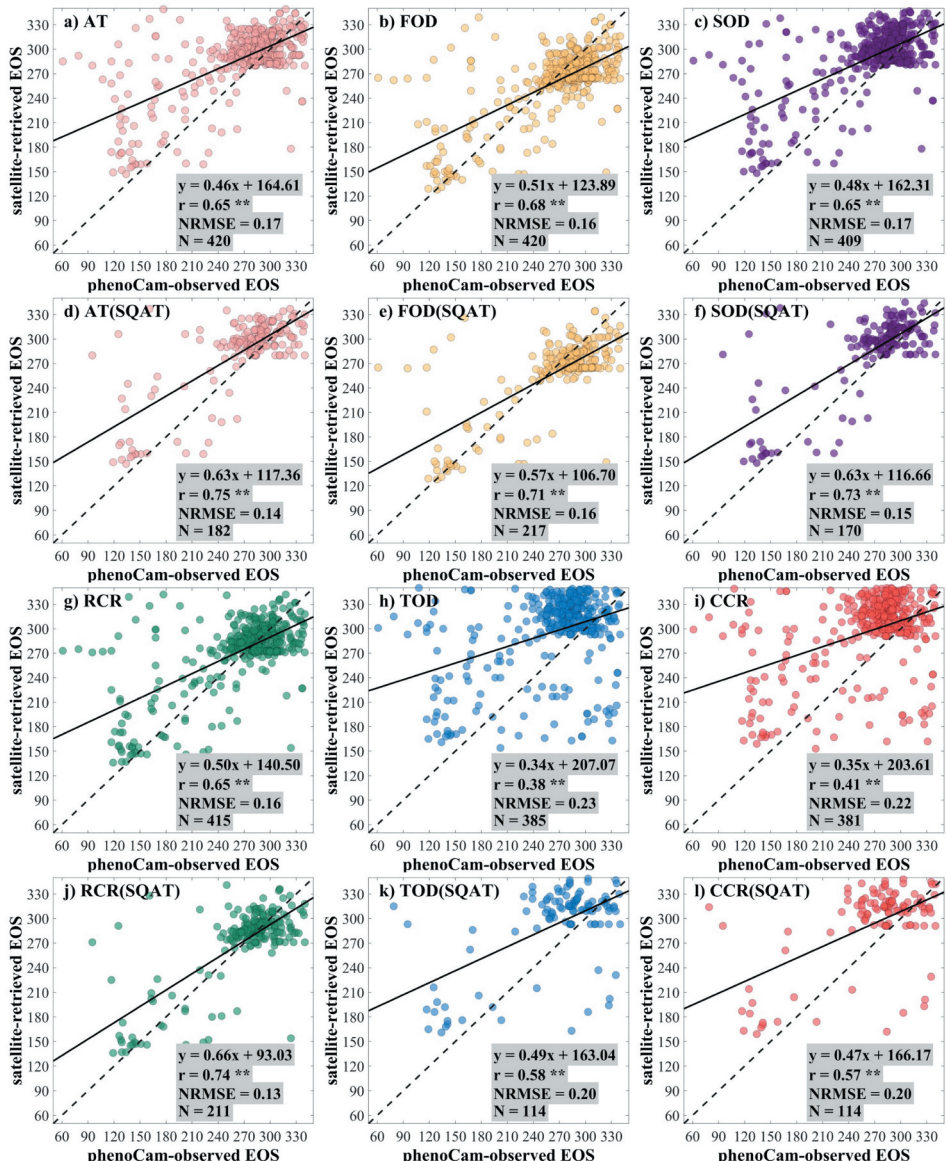


**Figure 5.** Scatterplots for the regression analysis between the PhenoCam-observed and satellite-retrieved EOS using the methods of: (a) Amplitude threshold (AT); (b) first-order derivative (FOD); (c) second-order derivative (SOD); (d) AT and the shape quality assurance score threshold (SQAT); (e) FOD and SQAT; (f) SOD and SQAT; (g) relative change rate (RCR); (h) third-order derivative (TOD); (i) curvature change rate (CCR); (j) RCR and SQAT; (k) TOD and SQAT; and (l) CCR and SQAT. SQAT denotes use of the SQAT method for quality management of satellite-retrieved EOS. \*\* denotes a  $p$ -value of two-tailed Student's  $t$ -tests of  $<0.01$ . N denotes the number of validation sites.

pixels near North Dakota, South Dakota, Nebraska, Iowa, and Illinois compared to Figure 8c and Figure 8e, respectively.

The spatial distribution for the EOS in 2017, including the estimated results by AT and FOD and the acquired results from MCD12Q2, is shown in Figure 9. Comparing with Figure

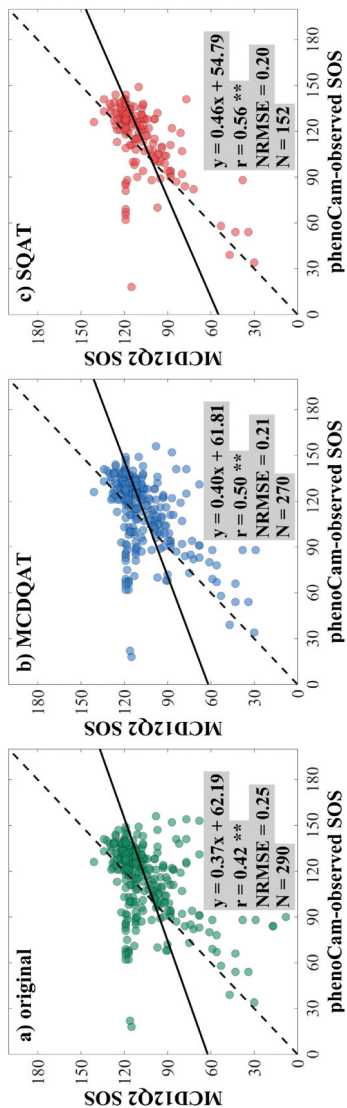


**Figure 6.** Scatterplots for comparison between the PhenoCam-observed SOS and (a) the original SOS of MCD12Q2, (b) the SOS of MCD12Q2 and using the best level threshold of the QA scores from MCD12Q2 (MCDQAT) for quality management, and (c) the SOS of MCD12Q2 and using the shape quality assurance score threshold (SQAT) for quality management. \*\* denotes a  $p$ -value of two-tailed Student's  $t$ -tests of  $<0.01$ .  $N$  denotes the number of validation sites.

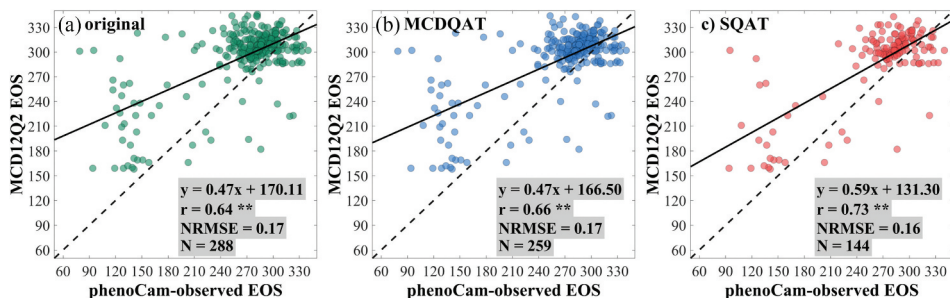


**Figure 7.** Scatterplots for comparison between the PhenoCam-observed EOS and (a) the original EOS of MCD12Q2, (b) the EOS of MCD12Q2 and using the best level threshold of the QA scores from MCD12Q2 (MCDQAT) for quality management, and (c) the EOS of MCD12Q2 and using the shape quality assurance score threshold (SQAT) for quality management. \*\* denotes a *p*-value of two-tailed Student's *t*-tests of <0.01. N denotes the number of validation sites.

9a, a few outlier pixels near Washington, Idaho, and Montana were removed by the MCDQAT method, while the other areas seem to be unchanged (Figure 9b). Using the SQAT method, the number of low-value (green) and high-value (red) pixels of the EOS maps in Figure 9d and Figure 9f are significantly decreased, especially for the red pixels. The SOS (or EOS) uses SQAT for quality management, the removed pixels are mainly consisting of high value or low value. The results indicate that the SQAT method can effectively remove outlier pixels at a regional scale.

## 5. Discussion

In this paper, we proposed a SQAT method for quality management of the vegetation phenophases derived from satellite-derived vegetation index. The main idea behind SQA is to improve the MCD12Q2 QA method by further considerations on the trends in satellite-derived vegetation index associated with the process of vegetation growth. SQAT method evaluates the quality of the vegetation phenophases according to the goodness-of-fit, the proportion of high-quality pixels and the tendency of vegetation growth. It is independent with the used data products and phenology extraction algorithms. Therefore, it can be used to deal with any other optical satellite sensor data, such as Advanced Very High-Resolution Radiometer (AVHRR), Landsat and Sentinel 2A/B data. It is also applicable to optimize the phenophases derived from different algorithms (e.g. AT, FOD, SOD, RCR, TOD and CCR). The SQAT method proposed in this paper is recommended to be used for quality management of vegetation phenophases in the northern hemisphere, as the effectiveness SQAT method is only evaluated in the conterminous United States (northern hemisphere). The performance of SQAT method in southern hemisphere region still needs further evaluation. We used Phenocam dataset to evaluate the performance of the SQAT method, and Phenocam dataset mainly tracks phenophases for natural vegetation such as forest, grassland, and shrub, which normally includes only a single growth peak. The proposed method might also be effective for vegetation types with multiple growth peaks, which will be further investigated in the near future.

Because the QA window was set as 2 weeks before and after the vegetation phenophase (i.e. SOS and EOS) (Friedl, Gray, and Sulla-Menashe 2019), the SQAT method can be

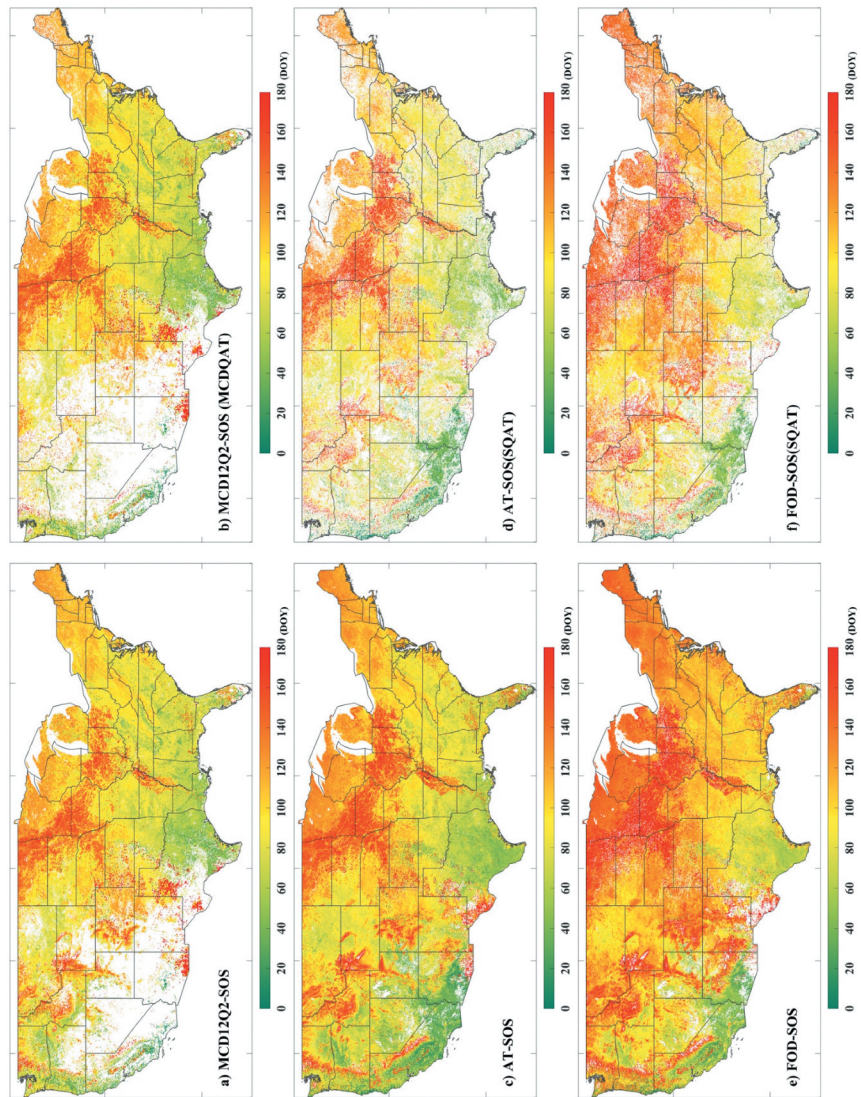


**Figure 8.** Spatial distribution for the start of season (SOS) in 2017, (a) the SOS acquired from MCD12Q2; (b) the SOS acquired from MCD12Q2 and quality management by MCDQAT; (c) the SOS derived from MOD09Q1 EV12 by the amplitude threshold (AT); (d) the SOS derived from MOD09Q1 EV12 by AT and quality management by shape quality assurance score threshold (SQAT); (e) the SOS derived from MOD09Q1 EV12 by the first-order derivative (FOD); and (f) the SOS derived from MOD09Q1 EV12 by FOD and quality management by SQAT across the conterminous United States. The embedded subplots show the removed pixels of the MCD12Q2-SOS, AT-SOS, and FOD-SOS by quality management of MCDQAT or SQAT.

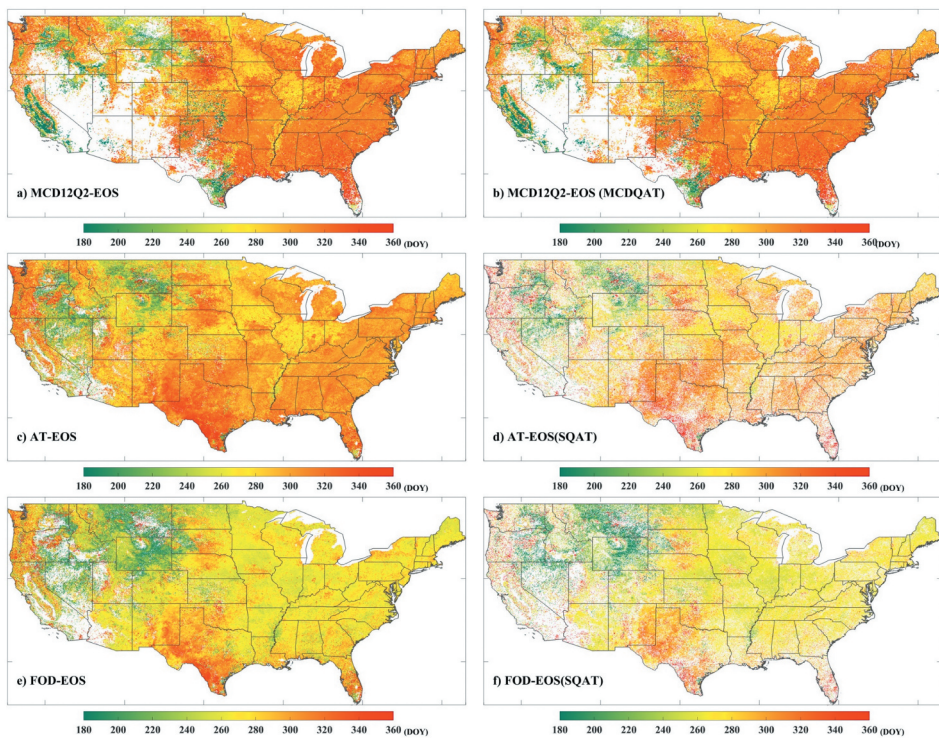


**Figure 9.** Spatial distribution for the end of season (EOS) in 2017, (a) the EOS acquired from MCD12Q2; (b) the EOS acquired from MCD12Q2 and quality management by MCDQAT; (c) the EOS derived from MOD09Q1 EVI2 by the amplitude threshold (AT); (d) the EOS derived from MOD09Q1 EVI2 by AT and quality management by shape quality assurance score threshold (SQAT); (e) the EOS derived from MOD09Q1 EVI2 by the first-order derivative (FOD); and (f) the EOS derived from MOD09Q1 EVI2 by FOD and quality management by SQAT across the conterminous United States. The embedded subplots show the removed pixels of the MCD12Q2-EOS, AT-EOS, and FOD-EOS by quality management of MCDQAT or SQAT.

used effectively for the vegetation phenophase between 14<sup>th</sup> day to 351<sup>th</sup> day of the year. Generally, the SOS of vegetation is later than 14<sup>th</sup> day of the year, while EOS is earlier than 351<sup>th</sup> day of the year. For instance, Zhou et al. (2016) excluded the pixels value with the SOS earlier than the 50<sup>th</sup> day of year or later than the 180<sup>th</sup> day of year for the SOS analysis, and they only constrained the EOS between the 240<sup>th</sup> and 330<sup>th</sup> day of year in the China research region; Li et al. (2017) made slightly adjustment to Zhou et al. (2016) that the terms of these thresholds with a temporal lag of 20 days in the conterminous United States research region. Therefore, in a special area where the SOS of vegetation is before than 14<sup>th</sup> day of the year, and EOS is after than 351<sup>th</sup> day of the year, we can conduct a special treatment by extending the time series of EVI2 for calculating the SQA score.

To keep consistent with the MCD12Q2 QA method, we adopted a SQA threshold of 0.75 in the experiments. We analysed the sensitivity of threshold by comparing the performance of different SQA thresholds with a constant MCD12Q2 QA threshold of 0.75. The evaluated SQA thresholds are in the range of 0.5 to 0.95, with an increment of 0.01. Results in Figure 10 shows that and the NRMSE value of SOS decreases significantly

when the SQA threshold changes from 0.5 to 0.86, and increases dramatically as the SQA threshold continues to increase. The possible reason may be that the too many points are removed by a large threshold. This phenomenon can also be observed in the EOS results. The MCDQAT method obtained slightly better results than the SQAT method when the threshold near 0.5, and the relationship reverses while the threshold near or greater than 0.75. Overall, the SQAT method can obtain a better result when the threshold is greater than 0.75.

In our experiment, we found notable differences between the ground-observed vegetation phenophases and the satellite-retrieved vegetation phenophases, which might have resulted from:

- (a) Remote-sensing data quality of satellite observations. The remote-sensing data used to monitor vegetation phenology is mainly from optical satellites. However, the quality of optical satellite remote-sensing data is easily affected by cloud and rain weather, which will directly affect the vegetation phenophases.
- (b) The quality of ground vegetation phenology observation records. The ground vegetation phenology records are widely come from manual observation or digital camera observation. However, the manual observation is subjective and the digital camera observation is easily affected by weather conditions and vegetation phenology retrieved algorithms.
- (c) The region of satellite observations might be inconsistent with ground observations. While using the ground observations to evaluate vegetation phenology retrieved from the satellite data, the position of the selected pixel in the satellite image is necessarily consistent with the position of the ground observation. However, the resolution of satellite image such as MOD09Q1 is about 250 m, and there is a noticeable mixed pixel phenomenon. The value of each pixel represents the average phenophase in a large area covering different types of vegetation. The ground observation by human is usually observing one or several plants, while the observation by the digital camera is selecting a specific plant of

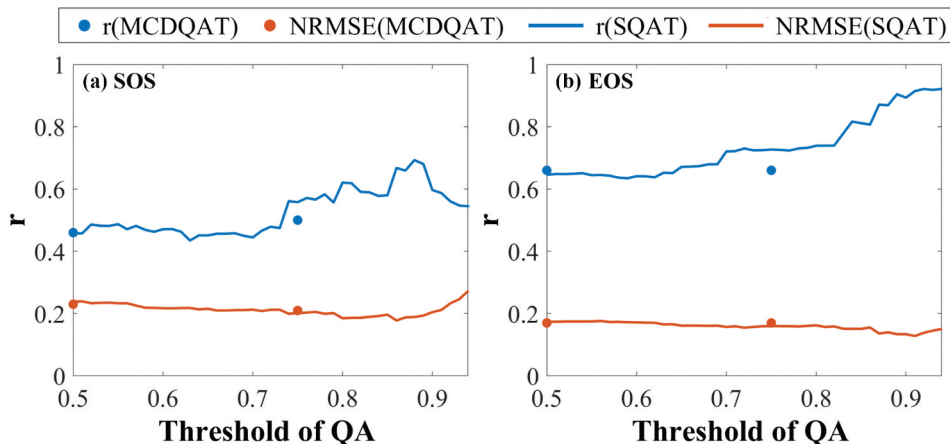


**Figure 10.** An illustration of the  $r$  value and NRMSE value change with the quality assurance score (QA) which are shown for (a) the start of season (SOS) and (b) the end of season (EOS).



the interest region in a camera photo. The scale effect could influence the validation of accuracy.

- (d) There is a spectral difference between satellite observations and digital camera observations in vegetation phenology. The spectrum of the digital camera is mostly equipped with three bands (red band, green band, and blue band) and the vegetation phenology often retrieved by the green chromatic coordinate index ( $G_{cc}$ ). However, the vegetation phenophases retrieved from satellite images are using red band and near-infrared band for vegetation indices calculation.

The increasing publicly available field observation data of the vegetation phenology provide sufficient training samples and make machine learning methods (such as neural networks, random forests, SVM, etc.) possible for vegetation phenology extraction from remote sensing data (Capinha 2019; Czernecki, Nowosad, and Katarzyna 2018; Xin et al. 2020). Studies have concluded that the machine learning models outperforms traditional methods when compared with field observation. Nevertheless, there are also situations that machine learning models does not perform well (Xin et al. 2020). SQAT method provides an effective method for quality management, which might be useful in optimize the results extracted by machine learning methods.

## 6. Conclusion

Here, we employed MOD09Q1, MCD12Q2, and PhenoCam-observed data to test the six widely used methods (i.e. amplitude threshold, first-order derivative, second-order derivative, relative change rate, third-order derivative, and curvature change rate) to estimate vegetation phenophases from satellite remote sensing data. The performance of the six methods in estimating SOS and EOS from MOD09Q1 EVI2 is stable. We proposed a SQAT quality management method, which has greatly improved the estimated start of season (SOS) and end of season (EOS) of the six methods (averagely increased r value by 8% for SOS, and 11% for EOS). When selecting the threshold of SQA, it is important to balance the accuracy and the remaining points. We adopted a SQA threshold of 0.75 in the experiments and found that the SQAT method can yield much better results than MCD12Q2 QA method. Using the SQAT method for quality management can reduce the uncertainty of vegetation phenology datasets, and can be helpful for models that use phenology datasets as input data.

## Acknowledgments

This research is supported by National Key R&D Program of China (grant no. 2018YFB2100702), National Natural Science Foundation of China (grant nos. 42,071,441 and 41,875,122), Hunan Botong Information Co. Ltd. grant no. BTZH2018001), the Smart Guangzhou Spatio-temporal Information Cloud Platform Construction (grant no. GZIT2016-A5-147), Western Talent (grant no. 2018XBYJRC004), and Guangdong Top Young Talents of Science and Technology (grant no. 2017TQ04Z359). We thank the MOD09Q1 data, MCD12Q2 data and PhenoCam data production researcher. We thank anonymous reviewers for their constructive comments.

## Data availability

The MODIS/Terra surface reflectance 8-day 250 m product (MOD09Q1, Version 6) was available from <https://search.earthdata.nasa.gov/>. The MODIS/Terra and Aqua Land Cover Dynamics Yearly L3 Global 500 m SIN Grid (MCD12Q2, Version 6) was available from <https://search.earthdata.nasa.gov/>. The PhenoCam Dataset v2.0 was obtained (<https://phenocam.sr.unh.edu/webcam/>) for validation.

## Disclosure of potential conflicts of interest

No potential conflict of interest was reported by the author(s).

## Funding

This work is supported by National Key R&D Program of China [2018YFB2100702], National Natural Science Foundation of China [42071441, 41875122], Hunan Botong Information Co. Ltd. [BTZH2018001], the Smart Guangzhou Spatio-temporal Information Cloud Platform Construction [GZIT2016-A5-147], Western Talent [2018XBYJRC004], and Guangdong Top Young Talents of Science and Technology [2017TQ04Z359].

## ORCID

Qinchuan Xin  <http://orcid.org/0000-0003-1146-4874>

## References

- Capinha, C. 2019. "Predicting the Timing of Ecological Phenomena Using Dates of Species Occurrence Records: A Methodological Approach and Test Case with Mushrooms." *International Journal of Biometeorology* 63 (8): 1015–1024. doi:[10.1007/s00484-019-01714-0](https://doi.org/10.1007/s00484-019-01714-0).
- Czernecki, B., J. Nowosad, and J. Katarzyna. 2018. "Machine Learning Modeling of Plant Phenology Based on Coupling Satellite and Gridded Meteorological Dataset." *International Journal of Biometeorology* 62 (7): 1297–1309. doi:[10.1007/s00484-018-1534-2](https://doi.org/10.1007/s00484-018-1534-2).
- Fischer, A. 1994. "A Model for the Seasonal Variations of Vegetation Indices in Coarse Resolution Data and Its Inversion to Extract Crop Parameters." *Remote Sensing of Environment* 48 (2): 220–230. doi:[10.1016/0034-4257\(94\)90143-0](https://doi.org/10.1016/0034-4257(94)90143-0).
- Friedl, M., J. Gray, and D. Sulla-Menashe. 2019. "MCD12Q2 MODIS/Terra+Aqua Land Cover Dynamics Yearly L3 Global 500m SIN Grid V006." NASA EOSDIS Land Processes DAAC. doi:[10.5067/MODIS/MCD12Q2.006](https://doi.org/10.5067/MODIS/MCD12Q2.006).
- Fu, Y. H., H. Zhao, S. Piao, M. Peaucelle, S. Peng, G. Zhou, P. Ciais, et al. 2015. "Declining Global Warming Effects on the Phenology of Spring Leaf Unfolding." *Nature* 526 (7571): 104–107. doi:[10.1038/nature15402](https://doi.org/10.1038/nature15402).
- Ge, Q., H. Wang, T. Rutishauser, and J. Dai. 2015. "Phenological Response to Climate Change in China: A Meta-analysis." *Global Change Biology* 21 (1): 265–274. doi:[10.1111/gcb.12648](https://doi.org/10.1111/gcb.12648).
- Hufkens, K., D. Basler, E. K. Tom Milliman, Melaas, A. D. Richardson, and A. D. Melaas. 2018. "An Integrated Phenology Modelling Framework in R." *Methods in Ecology and Evolution* 9 (5): 1276–1285. doi:[10.1111/2041-210X.12970](https://doi.org/10.1111/2041-210X.12970).
- Jiang, Z. Y., A. R. Huete, K. Didan, and T. Miura. 2008. "Development of a Two-band Enhanced Vegetation Index without a Blue Band." *Remote Sensing of Environment* 112 (10): 3833–3845. doi:[10.1016/j.rse.2008.06.006](https://doi.org/10.1016/j.rse.2008.06.006).
- Jun, L., L. Chian-Yi, T. J. Huang Hung-Lung, W. X. Schmit, W. P. Menzel, J. J. Gurka, and J. J. Gurka. 2005. "Optimal Cloud-clearing for AIRS Radiances Using MODIS." *IEEE Transactions on Geoscience and Remote Sensing* 43 (6): 1266–1278. doi:[10.1109/TGRS.2005.847795](https://doi.org/10.1109/TGRS.2005.847795).



- Kuklisova-Murgasova, M., M. A. Gerardine Quaghebeur, J. V. Rutherford, Hajnal, J. A. Schnabel, and J. A. Hajnal. 2012. "Reconstruction of Fetal Brain MRI with Intensity Matching and Complete Outlier Removal." *Medical Image Analysis* 16 (8): 1550–1564. doi:[10.1016/j.media.2012.07.004](https://doi.org/10.1016/j.media.2012.07.004).
- Latifovic, R., and D. Pouliot. 2007. "Analysis of Climate Change Impacts on Lake Ice Phenology in Canada Using the Historical Satellite Data Record." *Remote Sensing of Environment* 106 (4): 492–507. doi:[10.1016/j.rse.2006.09.015](https://doi.org/10.1016/j.rse.2006.09.015).
- Li, X., G. R. Yuyu Zhou, J. M. Asrar, L. Xiaoma, and L. Wenyu. 2017. "Response of Vegetation Phenology to Urbanization in the Conterminous United States." *Global Change Biology* 23 (7): 2818–2830. doi:[10.1111/gcb.13562](https://doi.org/10.1111/gcb.13562).
- Lucht, W. I., R. B. Colin Prentice, S. S. Myneni, P. Friedlingstein, W. Cramer, P. Bousquet, W. Buermann, and B. Smith. 2002. "Climatic Control of the High-Latitude Vegetation Greening Trend and Pinatubo Effect." *Science* 296 (5573): 1687. doi:[10.1126/science.1071828](https://doi.org/10.1126/science.1071828).
- Menzel, A. 2002. "Phenology: Its Importance to the Global Change Community." *Climatic Change* 54 (4): 379–385. doi:[10.1023/A:1016125215496](https://doi.org/10.1023/A:1016125215496).
- Myneni, R. B., C. D. Keeling, C. J. Tucker, G. Asrar, and R. R. Nemani. 1997. "Increased Plant Growth in the Northern High Latitudes from 1981 to 1991." *Nature* 386 (6626): 698–702. doi:[10.1038/386698a0](https://doi.org/10.1038/386698a0).
- Piao, S., J. Fang, L. Zhou, P. Ciais, and B. Zhu. 2006. "Variations in Satellite-derived Phenology in China's Temperate Vegetation." *Global Change Biology* 12 (4): 672–685. doi:[10.1111/j.1365-2486.2006.01123.x](https://doi.org/10.1111/j.1365-2486.2006.01123.x).
- Piao, S., P. Friedlingstein, P. Ciais, N. Viovy, and J. Demarty. 2007. "Growing Season Extension and Its Impact on Terrestrial Carbon Cycle in the Northern Hemisphere over the past 2 Decades." *Global Biogeochemical Cycles* 21 (3): 3. doi:[10.1029/2006GB002888](https://doi.org/10.1029/2006GB002888).
- Richardson, A. D., K. Hufkens, T. Milliman, D. M. Aubrecht, M. Chen, J. M. Gray, M. R. Johnston, et al. 2018. "Tracking Vegetation Phenology across Diverse North American Biomes Using PhenoCam Imagery." *Scientific Data* 5 (1): 180028. doi:[10.1038/sdata.2018.28](https://doi.org/10.1038/sdata.2018.28).
- Seyednasrollah, B., A. M. Young, K. Hufkens, T. Milliman, M. A. Friedl, S. Froliking, A. D. Richardson, et al. 2019. "PhenoCam Dataset v2.0: Vegetation Phenology from Digital Camera Imagery, 2000–2018." In.: ORNL Distributed Active Archive Center, Oak Ridge, Tennessee, USA. <https://doi.org/10.3334/ORNLDaac/1674>.
- Richardson, A. D., T. F. Keenan, M. Migliavacca, Y. Ryu, O. Sonnentag, and M. Toomey. 2013. "Climate Change, Phenology, and Phenological Control of Vegetation Feedbacks to the Climate System." *Agricultural and Forest Meteorology* 169: 156–173. doi:[10.1016/j.agrformet.2012.09.012](https://doi.org/10.1016/j.agrformet.2012.09.012).
- Ruan, Y., X. Zhang, Q. Xin, A. Zurui, and Y. Sun. 2019. "Enhanced Vegetation Growth in the Urban Environment across 32 Cities in the Northern Hemisphere." *Journal of Geophysical Research: Biogeosciences* 124 (12): 3831–3846. doi:[10.1029/2019JG005262](https://doi.org/10.1029/2019JG005262).
- Ruan, Y., Y. Qiu, Y. Xiaoqi, H. Guo, and B. Cheng. 2016. "Passive Microwave Remote Sensing of Lake Freeze-thaw over High Mountain Asia." Paper presented at the 2016 IEEE International Geoscience and Remote Sensing Symposium (IGARSS), 10-15 July 2016, Beijing, China. doi:[10.1109/IGARSS.2016.7729728](https://doi.org/10.1109/IGARSS.2016.7729728).
- Sakamoto, T., M. Yokozawa, H. Toritani, M. Shibayama, N. Ishitsuka, and H. Ohno. 2005. "A Crop Phenology Detection Method Using Time-series MODIS Data." *Remote Sensing of Environment* 96 (3): 366–374. doi:[10.1016/j.rse.2005.03.008](https://doi.org/10.1016/j.rse.2005.03.008).
- Savitzky, A., and M. J. E. Golay. 1964. "Smoothing and Differentiation of Data by Simplified Least Squares Procedures." *Analytical Chemistry* 36 (8): 1627–1639. doi:[10.1021/ac60214a047](https://doi.org/10.1021/ac60214a047).
- Sonnentag, O., K. Hufkens, A. M. Cory Teshera-Sterne, M. F. Young, B. H. Braswell, T. Milliman, J. O'Keefe, and A. D. Richardson. 2012. "Digital Repeat Photography for Phenological Research in Forest Ecosystems." *Agricultural and Forest Meteorology* 152: 159–177. doi:[10.1016/j.agrformet.2011.09.009](https://doi.org/10.1016/j.agrformet.2011.09.009).
- Tan, B., J. T. Morisette, R. E. Wolfe, F. Gao, G. A. Ederer, J. Nightingale, and J. A. Pedelty. 2011. "An Enhanced TIMESAT Algorithm for Estimating Vegetation Phenology Metrics from MODIS Data." *IEEE Journal of Selected Topics in Applied Earth Observations and Remote Sensing* 4 (2): 361–371. doi:[10.1109/JSTARS.2010.2075916](https://doi.org/10.1109/JSTARS.2010.2075916).

- Templ, B., E. Koch, K. Bolmgren, M. Ungersböck, A. Paul, H. Scheifinger, T. Rutishauser, et al. 2018. "Pan European Phenological Database (PEP725): A Single Point of Access for European Data." *International Journal of Biometeorology* 62 (6): 1109–1113. doi:[10.1007/s00484-018-1512-8](https://doi.org/10.1007/s00484-018-1512-8).
- Vermote, E. 2015. "MOD09Q1 MODIS/Terra Surface Reflectance 8-Day L3 Global 250m SIN Grid V006." *NASA EOSDIS Land Processes DAAC*. doi:[10.5067/MODIS/MOD09Q1.006](https://doi.org/10.5067/MODIS/MOD09Q1.006).
- Wang, X., H. Xie, and T. Liang. 2008. "Evaluation of MODIS Snow Cover and Cloud Mask and Its Application in Northern Xinjiang, China." *Remote Sensing of Environment* 112 (4): 1497–1513. doi:[10.1016/j.rse.2007.05.016](https://doi.org/10.1016/j.rse.2007.05.016).
- Weber, H., M. Riffler, T. Noges, and S. Wunderle. 2016. "Lake Ice Phenology from AVHRR Data for European Lakes: An Automated Two-step Extraction Method." *Remote Sensing of Environment* 174: 329–340. doi:[10.1016/j.rse.2015.12.014](https://doi.org/10.1016/j.rse.2015.12.014).
- Xin, Q., L. Jing, L. Ziming, L. Yaoming, and X. Zhou. 2020. "Evaluations and Comparisons of Rule-based and Machine-learning-based Methods to Retrieve Satellite-based Vegetation Phenology Using MODIS and USA National Phenology Network Data." *International Journal of Applied Earth Observation and Geoinformation* 93: 102189. doi:[10.1016/j.jag.2020.102189](https://doi.org/10.1016/j.jag.2020.102189).
- Xin, Q., M. Broich, P. Zhu, and P. Gong. 2015. "Modeling Grassland Spring Onset across the Western United States Using Climate Variables and MODIS-derived Phenology Metrics." *Remote Sensing of Environment* 161: 63–77. doi:[10.1016/j.rse.2015.02.003](https://doi.org/10.1016/j.rse.2015.02.003).
- Xin, Q., Y. Dai, and X. Liu. 2019. "A Simple Time-stepping Scheme to Simulate Leaf Area Index, Phenology, and Gross Primary Production across Deciduous Broadleaf Forests in the Eastern United States." *Biogeosciences* 16 (2): 467–484. doi:[10.5194/bg-16-467-2019](https://doi.org/10.5194/bg-16-467-2019).
- Yang, X., J. F. Mustard, J. Tang, and X. Hong. 2012. "Regional-scale Phenology Modeling Based on Meteorological Records and Remote Sensing Observations." *Journal of Geophysical Research: Biogeosciences* 117 (G3): G3. doi:[10.1029/2012JG001977](https://doi.org/10.1029/2012JG001977).
- Yu, F., K. P. Price, J. Ellis, and P. Shi. 2003. "Response of Seasonal Vegetation Development to Climatic Variations in Eastern Central Asia." *Remote Sensing of Environment* 87 (1): 42–54. doi:[10.1016/S0034-4257\(03\)00144-5](https://doi.org/10.1016/S0034-4257(03)00144-5).
- Zhang, X., M. A. Friedl, C. B. Schaaf, A. H. Strahler, C. F. John, F. G. Hodges, B. C. Reed, and A. Huete. 2003. "Monitoring Vegetation Phenology Using MODIS." *Remote Sensing of Environment* 84 (3): 471–475. doi:[10.1016/S0034-4257\(02\)00135-9](https://doi.org/10.1016/S0034-4257(02)00135-9).
- Zhou, D., S. Zhao, L. Zhang, and S. Liu. 2016. "Remotely Sensed Assessment of Urbanization Effects on Vegetation Phenology in China's 32 Major Cities." *Remote Sensing of Environment* 176: 272–281. doi:[10.1016/j.rse.2016.02.010](https://doi.org/10.1016/j.rse.2016.02.010).